DINAME 2017 - Proceedings of the XVII International Symposium on Dynamic Problems of Mechanics
A. T. Fleury, D. A. Rade, P. R. G. Kurka (Editors), ABCM, São Sebastião, SP, Brazil, March 5-10, 2017

Investigation of Motion Planning Methods with a Kinematically Redundant Manipulator

João Cavalcanti Santos [1], **Maíra Martins da Silva** [1]

[1] Escola de Engenharia de São Carlos - Universidade de São Paulo, joao.cavalcanti.santos@usp.br, mairams@sc.usp.br

Abstract: Kinematic redundancy is capable of enhancing dynamic performance, improving precision, applying obstacle avoidance, among others. Nevertheless, the academy does not present a well-established method for planning the motion of the additional degrees of freedom available with manipulators with this type of redundancy. In order to contribute to the fulfillment of this gap, different motion planning strategies for a kinematically redundant manipulator are compared through experimental tests and numerical simulations. A planar parallel manipulator 3PRRR is used as an example. Necessary mathematical models are introduced. The ability to maintain high precision and rigidity is analyzed. In addition, dynamic performance is improved through the reduction of actuator loads. A truncated solution which optimizes just initial and final positions presented limited efficiency thanks to the fact that it does not freely vary positions for each instant of the task. Inverse kinematic resolution attained high rigidity and precision, but demanded inconsistent forces. Finally, a global optimization which compromises with these characteristics and accelerations (demanding lower forces) proved to be an efficient algorithm.

Keywords: Parallel Kinematic Manipulators, Kinematic Redundancy, Motion Planning.

1. INTRODUCTION

The structure of a Parallel Kinematic Manipulator (PKM) is a closed loop mechanism which connects the base to the end-effector through several kinematic chains. This characteristic reduces the moving mass of the system and split the loads between its several kinematic chains. As a consequence, many enhancements over the serial architecture are possible. Mainly, the following improvements can be obtained: higher rigidity, dynamic performance and load capacity/robot mass ratio. Still, kinematic constraints for PKMs are more restrictive, reducing their workspace. In addition, singularities may be encountered where the mechanism rigidity is completely lost thanks to the presence of passive joints (Merlet, 2012).

In an effort to overcome these drawbacks, kinematic redundancy may be applied (Fontes and da Silva, 2016). Kinematic redundancy is defined as the introduction of extra active joints in a kinematic chain. A manipulator with this type of redundancy has higher mobility than the required by the number of degrees of freedom (DOF) of the end-effector. That is to say, the mechanism as a whole has more DOFs than the end-effector. Thus, these extra DOFs can be used in order to increase the workspace and avoid singularities. More specifically, kinematic redundancy makes the inverse kinematic undefined. For a given pose of the end-effector, there is an infinite set of possible positions of actuators. As a consequence, seeking a full benefit obtained from kinematic redundancy, one has to choose, among this infinite set, which is the best. This should be done for each instant during a task, resulting in a Motion Planning process. Motion planning for redundant manipulators can also be denoted as Redundancy Resolution (Ahuactzin and Gupta, 1999; Siciliano, 1990).

This problem is usually addressed locally, optimizing the inverse kinematics for each instant individually (Ozgoren, 2013; Siciliano, 1990; Xiang et al., 2010). In other words, for a given position of the manipulator and a given velocity of the end-effector, this method defines an optimum velocity of the actuators. As a result, the inverse kinematic becomes a defined mathematical relation, unlike the initial problem. This procedure is called inverse kinematic resolution.

Although, in many applications of automation, the complete path is previously known. Clearly, the aforementioned method does not use this privilege, inasmuch as joints velocities are optimized for each instant locally. Other methods have been proposed seeking a global optimum (Kazerounian and Wang, 1988; Agrawal and Xu, 1994). Unfortunately, these are known for requiring great computational efforts.

The present study exploits three motion planning strategies. The first, denoted as **Truncated Optimization**, is a truncated solution which seeks to minimize the maximum required torque of a chosen task, similar to the proposed in (Santos et al., 2015). The second algorithm, denoted as **Inverse Kinematic Resolution** (Siciliano, 1990), is a proposal based on the introduction of extra kinematic constraints that penalizes non-convenient positions. This solution may be inappropriate since it can lead to unfeasible motions. However, it can be used as reference to a global optimization problem able to consider technical limitations and imposed constraints. In this way, the third strategy considers the resulting motion of the Inverse Kinematic Resolution under a global point of view. This method, denoted here as **Global Optimization**, is

based on the aforementioned Inverse Kinematic Resolution algorithm. Using this strategy, the positions of each actuator can be found.

In this manuscript, the Global Optimization strategy is evaluated numerically and experimentally. To do so, a 3PRRR redundant manipulator is studied (see fig. 1). The description of this setup and its modeling is present in Sections 2 and 3, respectively. Motion planning strategies are introduced in Section 4. In Section 5, the numerical and experimental results are discussed. Conclusions are drawn in Section 6.

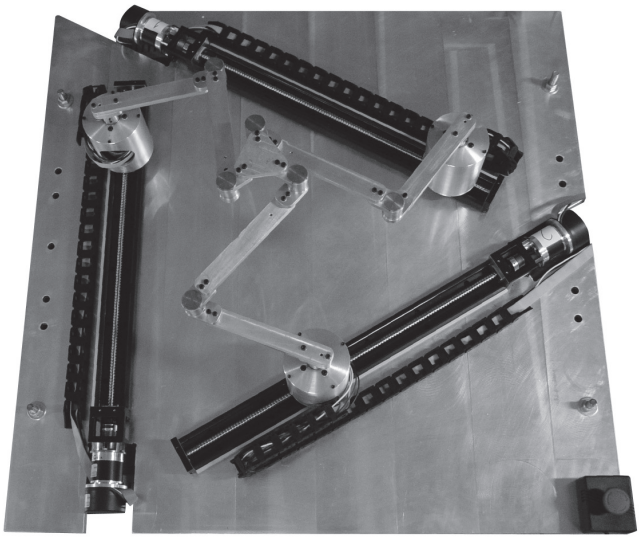

Figure 1: Prototype used for experimental tests

2. MANIPULATOR DESCRIPTION

Studies presented hereinafter are focused on a 3PRRR, a planar parallel robot with 3 kinematic chains. Each kinematic chain, i, presents a single prismatic joint (symbolized by P) and three revolute joints (symbolized by RRR). The prismatic and the first revolute joints are active (shown by the underlined letters). Figure 2 illustrates a schematic representation, indicating the kinematic parameters. The mechanism has 6 active joints, with its positions described by ζ_i and θ_i, where $i = 1,\ldots,3$ standing for each kinematic chain. On the other hand, the end-effector, a rigid body moving through the plane, has 3 DOFs, corresponding to the coordinates x, y and α. Thus, the manipulator presents 3 levels of kinematic redundancy.

Experimental data have been attained using a 3PRRR prototype built at the Engineering School of São Carlos - University of São Paulo (see fig. 1). The structural parts, as the base and links, have been made of aluminium. The passive revolute joints are composed of a pair of concentric ball bearings mounted in an outer structure made of aluminum.

The actuators responsible for the motion of the active joints are brushless rotary motors *Maxon EC60 flat*. The nominal speed and torque of these motors are 3580 rpm and 257 mN.m, respectively. These motors are coupled to planetary gearheads *Maxon GP 52 C*, with reduction ratio 3.5:1.

Each active revolute joint, θ_i, is actuated by this motor-gearhead set. Similarly, each active prismatic joint, ζ_i, is actuated by this motor-gearhead set coupled to a robotic table system with a ball screw *Hiwin KK60-10-C-E-600-A-1-F0-S3*. The stroke and pitch of this robotic table is 600 and 10mm, respectively. This assembly guarantees high precision and adequate reduction ratio

Every motor is controlled with an individual controller board *Maxon EPOS2 50/5*, with 5A of nominal direct current and 50VDC of maximum voltage. Many control methods are available with this equipment. Presented tests make use of the *Interpolated Position Mode*. In this mode, the user provides sets of information containing position, velocity and time step for multiple instants. The controller board, interpolating these points with splines, constructs a reference with the resulting curve. Position control is applied, using both linear feedforward and feedback signals. Controller parameters have been adjusted manually.

Geometric parameters of the manipulator 3PRRR are depicted in Fig. 2. Lengths of links A_iB_i and B_iC_i are, respectively, denoted by l_2 and l_3. Angles γ_i represent the orientation of each prismatic joint. Points B_i and C_i are passive revolute joints. Length h is the distance between the center of the end-effector and any point C_i. Distance between the center of the manipulator (which defines the origin of the coordinate system (x,y)) and the center of any linear actuator is a. The orientation of a link B_iC_i is β_i. Regarding the prototype dimensions, the numerical values of h, a, l_2 and l_3 are presented in Table 1. These same values have been used in simulations.

Table 1: Dimensions of the prototype

h	a	l_2	l_3
59.7 mm	259.8 mm	191 mm	232 mm

3. KINEMATIC AND DYNAMIC MODELS

Essential for simulations and the Redundancy Resolution, kinematic and dynamic models are presented in Sections 3.1 and 3.2. Both inverse and forward models are deduced.

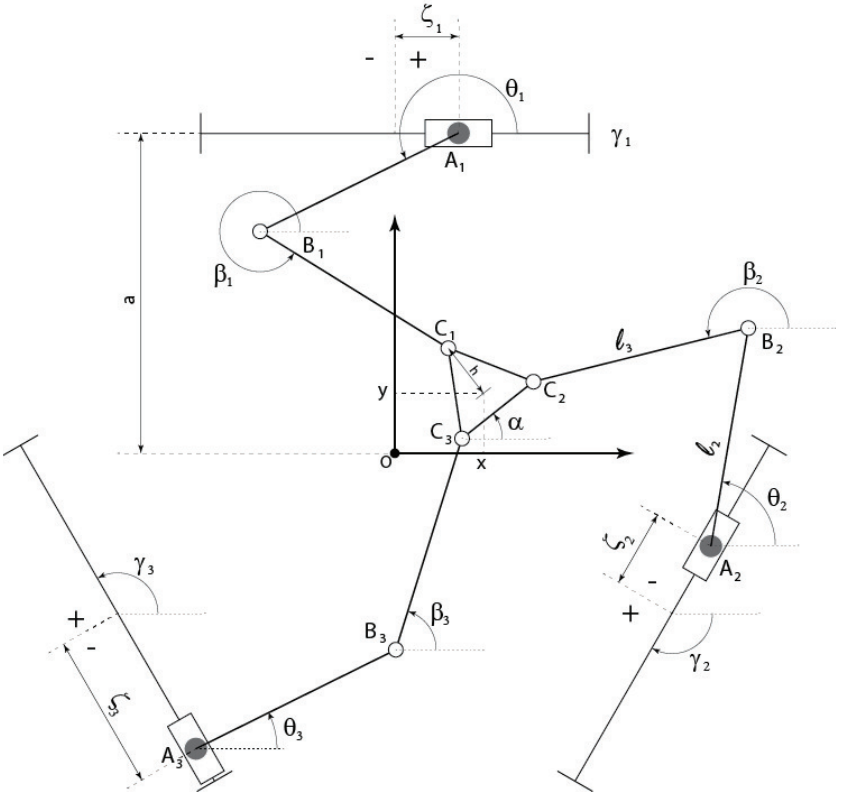

Figure 2: Schematic representation of 3PRRR

3.1 Kinematic Model

The present section develops relevant kinematic relations and parameters. Following the notation introduced earlier, section 3.1.1 deduces inverse and forward kinematics. In addition, the Jacobian matrix is defined in section 3.1.2. This matrix is used on motion planning methods and dynamic model.

3.1.1 Inverse and Forward Kinematics

The role of the kinematic model is to correlate actuator positions $\mathbf{\Theta} = [\theta_1, \theta_2, \theta_3, \zeta_1, \zeta_2, \zeta_3]^T$ to end-effector positions $\mathbf{X} = [x, y, \alpha]^T$. The Inverse Kinematic takes place when $\mathbf{\Theta}$ is determined for a given $\mathbf{X}$. Due to the kinematic redundancy, the mechanism has more DOF's than the end-effector. Therefore, actuators positions $(\zeta_1, \zeta_2, \zeta_3, \theta_1, \theta_2, \theta_3)$ are undetermined for a given (x, y, α). With this in minds, linear actuators positions $(\zeta_1, \zeta_2, \zeta_3)$ are assumed to be previously determined by some motion planning method. Thus, $(\theta_1, \theta_2, \theta_3)$ should be obtained from $(\zeta_1, \zeta_2, \zeta_3, x, y, \alpha)$.

To do so, kinematic constraints of a chain i is written eliminating β_i through the following equation:

$$||\mathbf{r_{C_i}} - \mathbf{r_{B_i}}||^2 = \left\| \begin{bmatrix} \rho_{xi} - l_2 \cos\theta_i \\ \rho_{yi} - l_2 \sin\theta_i \end{bmatrix} \right\|^2 = l_3^2, \tag{1}$$

where

$$\begin{bmatrix} \rho_{xi} \\ \rho_{yi} \end{bmatrix} = \begin{bmatrix} x \\ y \end{bmatrix} + h \begin{bmatrix} \cos(\alpha + \gamma_i \pm \pi/2) \\ \sin(\alpha + \gamma_i \pm \pi/2) \end{bmatrix} - \zeta_i \begin{bmatrix} \cos\gamma_i \\ \sin\gamma_i \end{bmatrix} - a \begin{bmatrix} \cos(\gamma_i \pm \pi/2) \\ \sin(\gamma_i \pm \pi/2) \end{bmatrix}. \tag{2}$$

Vector $\mathbf{r_{OA_i}}$ are written as $a[\cos(\gamma_i \pm \pi/2)\ \sin(\gamma_i \pm \pi/2)]^T$ because its length is a and its orientation is perpendicular to the respective linear actuator given by γ_i. The signal of $\pm\pi/2$ is defined in function of the direction of increase of ζ_i.

For the specific case of Fig. 2, the angle is $\gamma_i + {}^{\pi}/_{2}$. The same rationale is employed for the vector which is the second parcel on the right-hand of (2).

Expanding the norm in (1):

$$\underbrace{-2.l_2.\rho_{yi}}_{e_{1i}} \sin\theta_i + \underbrace{-2.l_2.\rho_{xi}}_{e_{2i}} \cos\theta_i + \underbrace{\rho_{xi}^2 + \rho_{yi}^2 + l_2^2 - l_3^2}_{e_{3i}} = 0. \tag{3}$$

The transcendental equation (3) may be solved analytically θ_i with the *Weierstrass substitution*, transforming trigonometric functions of θ_i in functions of $\tan\left({}^{\theta_i}/_{2}\right)$, yielding:

$$\theta_i = 2\tan^{-1}\left(\frac{-e_{i1} \pm \sqrt{e_{i1}^2 + e_{i2}^2 - e_{i3}^2}}{e_{i3} - e_{i2}}\right). \tag{4}$$

Once θ_i is known, β_i can be found. It can be done through the following expression:

$$\beta_i = \tan^{-1}\left(\frac{\rho_{yi} - l_2 \sin\theta_i}{\rho_{xi} - l_2 \cos\theta_i}\right). \tag{5}$$

In general, available data regarding robot positions is limited to readings of $\mathbf{\Theta}$ given by encoders. This way, finding end-effector positions $\mathbf{X}$ for a given $\mathbf{\Theta}$ is required. This method is called Forward Kinematics. Mathematical complexity makes analytical methods difficult in this case. Therefore, this relation is attained numerically. For known ζ_i e θ_i ($i = 1,2,3$), equation (1) is solved numerically, defining x, y e α.

3.1.2 Jacobian Matrix

A relevant information of the manipulator for a given position is its Jacobian Matrix. It can be derived from the equation $||\mathbf{r_{BC}}||^2 = l_3^2$. Its derivative is $r_{BC_x}\dot{r}_{BC_x} + r_{BC_y}\dot{r}_{BC_y} = 0$. Position elements r_{BC_x} e r_{BC_y} are substituted by $l_3\cos\beta_i$ e $l_3\sin\beta_i$, respectively. Velocity components $\dot{r}_{BC_x}$ and $\dot{r}_{BC_y}$ are obtained differentiating (3). Thus, the evaluation of each kinematic chain i leads to the following relation:

$$\dot{x}\underbrace{[l_3\cos\beta_i]}_{a_{i1}} + \dot{y}\underbrace{[l_3\sin\beta_i]}_{a_{i2}} + \dot{\alpha}\underbrace{[l_3\, h\sin(\beta_i - \gamma_i - \alpha \pm {}^{\pi}/_{2})]}_{a_{i3}} = \dot{\theta}_i\underbrace{[l_2\, l_3\sin(\beta_i - \theta_i)]}_{b_{ii}} + \dot{\zeta}_i\underbrace{[l_3\cos(\beta_i - \gamma_i)]}_{b_{ii+3}} \tag{6}$$

Following the sub-indices as described in (6), matrices $\mathbf{A}_{3x3} = (a_{i,j})$ and $\mathbf{B}_{3x6} = (b_{i,j})$ can be assembled so that $\mathbf{X} = [x, y, \alpha]^T$ and $\mathbf{\Theta} = [\theta_1, \theta_2, \theta_3, \zeta_1, \zeta_2, \zeta_3]^T$ have their velocities correlated by

$$\begin{aligned} \mathbf{A}_{3x3}\dot{\mathbf{X}}_{3x1} &= \mathbf{B}_{3x6}\dot{\mathbf{\Theta}}_{6x1} \\ \dot{\mathbf{X}} &= \mathbf{A}^{-1}\mathbf{B}\dot{\mathbf{\Theta}} \end{aligned} \tag{7}$$

In this way, the Jacobian Matrix $\mathbf{J}_{3x6}$ is calculated as $\mathbf{J} = \mathbf{A}^{-1}\mathbf{B}$. It is important to note that the occurrence of $\mathbf{A}$ or $\mathbf{B}$ with null determinant leads to singularities. The major concern regarding this matter is in cases when $\mathbf{A}$ is singular, making possible displacements of $\mathbf{X}$ with actuators locked. This situation induces a loss of rigidity of the mechanism.

3.2 Dynamic Model

Additionally to the Kinematic Model, the complete assessment of the system performance via simulations requires the development of a Dynamic Model. This model is built analytically and numerical methods able to solve it are proposed. The Euler-Lagrange formalism has been used with Lagrange multipliers in order to account for kinematic constraints. Considering this strategy, the solution of a set of Differential Algebraic Equations (DAE) is necessary. This is performed via numerical integration of the Forward Dynamics. The method proposed by (Brenan et al., 1996) has been implemented, using *Backward Differential Formula* (BDF) for this integration.

3.2.1 Mass Matrix and Kinematic Energy

For a kinematic chain i, position parameters are $\mathbf{\Theta}_i^* = [\zeta_i\ \theta_i\ \beta_i]^T$, according to Fig.2. The indication * displays that the original vector of actuator positions has been augmented with the orientation of the passive joint β_i. Each chain has three rigid bodies, which can be identified by an index j as follows: ($j = 1$) the body considered as a concentrated mass in A_i, ($j = 2$) the link $\overline{A_iB_i}$, and ($j = 3$) the link $\overline{B_iC_i}$.

The vector $\boldsymbol{\nu}_{ij}$ related to body j of chain i presents its Cartesian and rotational velocities $\boldsymbol{\nu}_{ij} = [v_{x_{ij}}\ v_{y_{ij}}\ \omega_{ij}]^T$ where $v_{x_{ij}}$ and $v_{y_{ij}}$ are Cartesian velocities of the center of mass in x and y respectively and ω_{ij} is the angular velocity.

It is necessary to define matrices that relate $\dot{\mathbf{\Theta}}_i^*$ to $\boldsymbol{\nu}_{ij}$. These matrices are called partial velocity matrices denoted by $\mathbf{K}_{ij}$:

$$
\begin{aligned}
\boldsymbol{\nu}_{i1} &= \underbrace{\begin{pmatrix} \cos\gamma_i & 0 & 0 \\ \sin\gamma_i & 0 & 0 \\ 0 & 0 & 0 \end{pmatrix}}_{\mathbf{K}_{i1}} \dot{\boldsymbol{\Theta}}_i^* \\
\boldsymbol{\nu}_{i2} &= \underbrace{\begin{pmatrix} \cos\gamma_i & -s_2\sin\theta_i & 0 \\ \sin\gamma_i & s_2\cos\theta_i & 0 \\ 0 & 1 & 0 \end{pmatrix}}_{\mathbf{K}_{i2}} \dot{\boldsymbol{\Theta}}_i^* \\
\boldsymbol{\nu}_{i3} &= \underbrace{\begin{pmatrix} \cos\gamma_i & -l_2\sin\theta_i & -s_3\sin\beta_i \\ \sin\gamma_i & l_2\cos\theta_i & s_3\cos\beta_i \\ 0 & 0 & 1 \end{pmatrix}}_{\mathbf{K}_{i3}} \dot{\boldsymbol{\Theta}}_i^*
\end{aligned}
\tag{8}
$$

where s_2 is the distance between A_i and the center of mass of link $\overline{A_iB_i}$, and s_3 is the distance between B_i and the center of mass of link $\overline{B_iC_i}$.

Let μ_j be a matrix with the parameters of a body j:

$$
\mu_j = \begin{pmatrix} m_j & 0 & 0 \\ 0 & m_j & 0 \\ 0 & 0 & I_j \end{pmatrix}, \tag{9}
$$

then T_i, the sum of kinetic energy of all bodies of the chain i is given by:

$$
\begin{aligned}
T_i &= \frac{1}{2}\sum_{j=1}^{3} \boldsymbol{\nu}_{ij}^T \mu_j \boldsymbol{\nu}_{ij} \\
&= \frac{1}{2}\dot{\boldsymbol{\Theta}}_i^{*T} \underbrace{\left(\sum_{j=1}^{3} \mathbf{K}_{ij}^T \mu_j \mathbf{K}_{ij}\right)}_{\mathbf{M}_i} \dot{\boldsymbol{\Theta}}_i^*.
\end{aligned}
\tag{10}
$$

In addition, the kinematic energy of the end-effector is:

$$
T_N = \frac{1}{2}\dot{\mathbf{X}}^T \underbrace{\begin{pmatrix} m_N & 0 & 0 \\ 0 & m_N & 0 \\ 0 & 0 & I_N \end{pmatrix}}_{\mathbf{M}_N} \dot{\mathbf{X}}. \tag{11}
$$

In order to assess total kinematic energy, a vector $\mathbf{q} = [\boldsymbol{\Theta}_1^{*T}\ \boldsymbol{\Theta}_2^{*T}\ \boldsymbol{\Theta}_3^{*T}\ \mathbf{X}^T]^T$ is defined so that:

$$
T = \frac{1}{2}\dot{\mathbf{q}}^T \mathbf{M} \dot{\mathbf{q}}, \tag{12}
$$

where the mass matrix $\mathbf{M}$ is fulfilled with submatrices $\mathbf{M}_1$, $\mathbf{M}_2$, $\mathbf{M}_3$ and $\mathbf{M}_N$ defined in (10) and (11) disposed as follows:

$$
\mathbf{M} = \begin{pmatrix} \mathbf{M}_1 & & & \\ & \mathbf{M}_2 & & \\ & & \mathbf{M}_3 & \\ & & & \mathbf{M}_N \end{pmatrix}. \tag{13}
$$

3.2.2 Dynamic Equations

Elements of vector $\mathbf{q}$ are not independent. The formulation of this dependence can be done through the Method of Lagrange Multipliers. Since the mechanism has 6 degrees of freedom while $\mathbf{q}$ has 12 components, 6 constraint equations together with 6 Lagrange multipliers should be applied. Constraint equations are:

$$
\begin{aligned}
\begin{bmatrix} g_p \\ g_{p+1} \end{bmatrix} =& a \begin{bmatrix} \cos(\gamma_i \pm \pi/2) \\ \sin(\gamma_i \pm \pi/2) \end{bmatrix} + \zeta_i \begin{bmatrix} \cos\gamma_i \\ \sin\gamma_i \end{bmatrix} + l_2 \begin{bmatrix} \cos\theta_i \\ \sin\theta_i \end{bmatrix} + \dots \\
&\dots + l_3 \begin{bmatrix} \cos\beta_i \\ \sin\beta_i \end{bmatrix} - h \begin{bmatrix} \cos(\alpha+\gamma_i \pm \pi/2) \\ \sin(\alpha+\gamma_i \pm \pi/2) \end{bmatrix} - \begin{bmatrix} x \\ y \end{bmatrix} = 0,
\end{aligned}
\tag{14}
$$

where $k = 2i$ and $i = 1,2,3$. See that each system of equations $[g_p \quad g_{p+1}]^T = 0$ represents kinematic constraints of a chain i, where $k = 2i$. This way, vectorial equation $\mathbf{g}_{6x1} = 0$ results in 6 algebraic equations.

Once there is not any variation of potential energy in this system (the robot moves in an horizontal plane), the lagrangian is $L = T$. Calculating partial and temporal derivatives of (12) and (14), the application of the Euler-Lagrange Equation with multiplier $\boldsymbol{\lambda} = [\lambda_1 \ \lambda_2 \ \dots \ \lambda_6]^T$ leads to

$$\begin{aligned} \mathbf{M}_{12x12}\,\ddot{\mathbf{q}}_{12x1} + \mathbf{b}_{12x1}(\mathbf{q},\dot{\mathbf{q}}) + \mathbf{G}^T\boldsymbol{\lambda} &= \boldsymbol{\tau} \quad (15) \\ \mathbf{g}(\mathbf{q}) &= 0. \quad (16) \end{aligned}$$

where $\mathbf{G}_{6x12}$ is the jacobian matrix of the vectorial function $\mathbf{g}$, $\boldsymbol{\tau} = [\tau_1 \ \tau_2 \ \dots \ \tau_{12}]^T$ has components τ_k representing non conservative generalized forces acting on q_k, and $\mathbf{b}$ is calculated by:

$$\mathbf{b}(\mathbf{q},\dot{\mathbf{q}}) = \dot{\mathbf{M}}\,\dot{\mathbf{q}} - \left[\frac{\partial T}{\partial q_1} \quad \frac{\partial T}{\partial q_2} \dots \frac{\partial T}{\partial q_{12}}\right]^T. \quad (17)$$

3.2.3 Inverse Dynamics

Knowing all positions $\mathbf{q}, \dot{\mathbf{q}}, \ddot{\mathbf{q}}$ over the time, Inverse Dynamics defines torques and forces necessary to perform such movement. One can see that unknown variables of (15) are $\boldsymbol{\lambda}$, τ_1, τ_2, τ_4, τ_5, τ_7 and τ_8 (τ_k, with lines k of eq. (15) related to ζ_i and θ_i). Lagrange multipliers $\boldsymbol{\lambda}$ are present in all 12 equations, while τ_k indicated above are present only in its respective equations $k = 1,2,4,5,7,8$. Therefore, remaining equations $k^c = 3,6,9,10,11,12$ have $\boldsymbol{\lambda}$ as unique unknown variable. With this in mind, $\boldsymbol{\lambda}$ can be isolated inverting the square matrix containing lines k^c of $\mathbf{G}^T$. After that, k components of $\boldsymbol{\tau}$ are obtained directly.

Equating this procedure, lines $k^c = 3,6,9,10,11,12$ are extracted from (15) (see that $\tau_{k^c} = 0$ when there is not any non conservative force in this components, that is to say, when these are frictionless passive joints)

$$\begin{aligned} \mathbf{M}_{k^c}\,\ddot{\mathbf{q}} + \mathbf{b}_{k^c} + \mathbf{G}_{k^c}^T\boldsymbol{\lambda} &= 0 \Rightarrow \\ \Rightarrow \boldsymbol{\lambda} &= -(\mathbf{G}_{k^c}^T)^{-1}(\mathbf{M}_{k^c}\,\ddot{\mathbf{q}} + \mathbf{b}_{k^c}) \quad (18) \end{aligned}$$

Substitution of (18) in (15) leads to forces and torques required from actuators τ_k.

Non conservative generalized forces (as disturbances and friction) acting in β_i, x, y and α can be easily added in (18) making $\tau_{k^c} \neq 0$. The simplest case where $\tau_{k^c} = 0$ has been exposed in an effort to facilitate comprehension.

3.2.4 Forward Dynamics

Forward Dynamics obtains the resulting movement $\mathbf{q}(t)$ knowing $\boldsymbol{\tau}(t)$. This takes place through numerical integration of the system (15/16). This is a system of Differential Algebraic Equations (DAE) with order 2 and index 3 (Hairer and Wanner, 1996). First of all, it is necessary to reduce its order to 1:

$$\begin{aligned} \mathbf{u} - \dot{\mathbf{q}} &= 0 \\ \mathbf{M}\,\dot{\mathbf{u}} + \mathbf{b}(\mathbf{q},\mathbf{u}) + \mathbf{G}^T\boldsymbol{\lambda} - \boldsymbol{\tau} &= 0 \quad (19) \\ \mathbf{g}(\mathbf{q}) &= 0 \end{aligned}$$

In order to integrate (19), *Backward Differential Formula* (BDF) has been used. This can approximate the derivatives $\dot{\mathbf{q}}(t_n)$ and $\dot{\mathbf{u}}(t_n)$ in a given instant t_n considering $\mathbf{q}$ and $\mathbf{u}$ calculated in previous steps. This way, unknown variables in (19) becomes $\mathbf{q}(t_n)$, $\mathbf{u}(t_n)$ and $\boldsymbol{\lambda}(t_n)$. Therefore, it can be solved as a purely algebraic system for each step. To do so, algorithm Trust Region Dogleg (built in MATLAB) has been used with the analytical jacobian matrix of the related system of algebraic equations.

It is noteworthy to say that this method is able to easily simulate disturbances and friction actuating in any part of the manipulator. Similarly, feedback control actions applied in an effort to suppress errors are simulated.

4. MOTION PLANNING

For a given pose of the end-effector, the kinematic redundancy yields to undetermined actuator positions. Using this idea, the present section focuses on the following problem: given an end-effector path $\mathbf{X}(t)$, define a convenient $\boldsymbol{\Theta}(t)$. Three different approaches are compared hereafter.

4.1 Truncated optimization

This first option truncates the problem of defining $\boldsymbol{\Theta}(t)$ for every instant into the optimization of the initial and final positions. Thus, input variables of the optimization are just $\boldsymbol{\Theta}(t_i)$ and $\boldsymbol{\Theta}(t_f)$, with t_i and t_f standing for initial and final instant, respectively. The function $\boldsymbol{\Theta}(t)$ is obtained from 5^{th} degree polynomials interpolating $\boldsymbol{\Theta}(t_i)$ and $\boldsymbol{\Theta}(t_f)$, with null velocities and accelerations on the beginning and the end of the task. The objective function is the maximum torque required, which is obtained through the dynamic model.

Since every position of the manipulator can be calculated with $\boldsymbol{\zeta}$ for a given position of the end-effector $\mathbf{X}$, this

problem can be stated as

$$\min_{\zeta^{\mathbf{i}}_{\mathbf{1,2,3}} \quad \zeta^{\mathbf{f}}_{\mathbf{1,2,3}}} ||\boldsymbol{\tau}||_\infty \tag{20}$$

$$s.t.$$

$$-\zeta_{max} \leq \zeta^{\mathbf{i}}_{\mathbf{1,2,3}} \leq \zeta_{max} \tag{21}$$

$$-\zeta_{max} \leq \zeta^{\mathbf{f}}_{\mathbf{1,2,3}} \leq \zeta_{max} \tag{22}$$

where ζ_{max} is related to amplitude constraints of linear actuators. The optimization above was solved using Sequential Quadratic Programming (SQP). This approach were studied in (Santos et al., 2015; Fontes et al., 2014), showing satisfying results with a 3PRRR.

4.2 Inverse Kinematic Resolution

Define a function $\phi(\boldsymbol{\zeta})$ which measures the quality of the position $\boldsymbol{\zeta}$ for a given end-effector position. This may include the rigidity, manipulability, proximity to constraints or obstacles, among others. Thus, a $\phi(\boldsymbol{\zeta})$ receives high values for convenient positions. With this in mind, a new kinematic constraint is added:

$$\dot{\boldsymbol{\zeta}} = \nabla\phi(\boldsymbol{\zeta}) \tag{23}$$

One can interpret that joint velocities points towards the most promising direction, according to ϕ. With this, the manipulator always tends to seek a better positioning. This resolutions is based on the method proposed in (Siciliano, 1990). References as (Xiang et al., 2010; Ozgoren, 2013) are examples of successful applications.

For the 3PRRR, the following aspects were addressed by $\phi(\boldsymbol{\zeta})$: (i) condition of the Jacobian matrix, (ii) limitation of amplitude of linear actuators and (iii) proximity to boundaries of the workspace.

4.3 Global optimization

Observe that the method in section 4.1 does not use the whole potential of the of the apparatus as a result of the truncation which takes place. Similarly, in section 4.2, the method disregard data related to future positions, since its input is just the instantaneous position. As a consequence, optimizing positions of each instant considering the whole task may present better results.

To do so, the inverse kinematic resolution (IKR) was used with ϕ multiplied by a constant with high value. This way, the velocity on eq. (23) receives values high enough to lead $\boldsymbol{\zeta}$ continuously to the optimum argument of $\phi(\boldsymbol{\zeta})$ in a given instant. Thus, the resulting motion obtained by the integration of (23) may be seen as a continuous profile presenting a locally optimum position for each instant.

However, parallel mechanisms typically present high variance of its dynamic performance over their workspace. As a result, this first optimum profile presents high accelerations in order to follow this variance. Then, this profile is used just as reference. The final motion is obtained through a global optimization compromising with the difference to this reference and its accelerations. Completing this procedure, the trade-off between a good positioning and low accelerations is attained.

This global optimization takes place using Differential Dynamic Programming, which is a well known method initially proposed in (Mayne, 1966). More specifically, naming $\boldsymbol{\zeta}_r$ the reference profile obtained through IKR and $\boldsymbol{\zeta}_o$ the final optimum profile, the algorithm described in (Tassa et al., 2012) was applied using a weighted sum of the acceleration $\ddot{\boldsymbol{\zeta}}$ and the difference $\boldsymbol{\zeta}_r - \boldsymbol{\zeta}_o$.

5. RESULTS

Methods presented in Section 4 are compared. Simulations shows that Truncated Optimization and the Inverse Kinematic Resolution are able to theoretically reduce torques and increase rigidity when neither disturbance nor uncertainty are considered. Nevertheless, both methods may fail in the presence of disturbances and uncertainties. The Global Optimization is able to overcome some of these problems.

Firstly, numerical results have been assessed for sake of comparison of the aforementioned strategies. To do so, a end-effector trajectory has been selected. This trajectory is obtained with a 5^{th} degree polynomial which interpolates initial and final positions with null accelerations and velocities. Initial and final positions are depicted in Fig. 3a. Considering the non-redundant 3RRR manipulator, this path presents a singularity. At this point, this motion required infeasible torque values and the Jacobian matrix is ill-conditioned. This yields to an important loss of rigidity.

The redundant manipulator 3PRRR should be capable of overcome this singularity region if an appropriate motion planning strategy is exploited. Numerically, the Truncated Optimization strategy have been able to plan the movement of the active joint reducing the nominal torque to a feasible value (0.43N.m). In spite of this promising numerical result, experimental tests demonstrate that the strategy fails to deliver robust results. The actual manipulator suffers from lack of rigidity not only at the singular point but nearby it. This aspect is not considered by the Truncated Optimization strategy, presenting a severe limitation. A simple way to evaluate this limitation is to simulate the system under disturbances. If the performance of the system is robust, the prototype is more likely to succeed. With this in mind, the forward dynamic

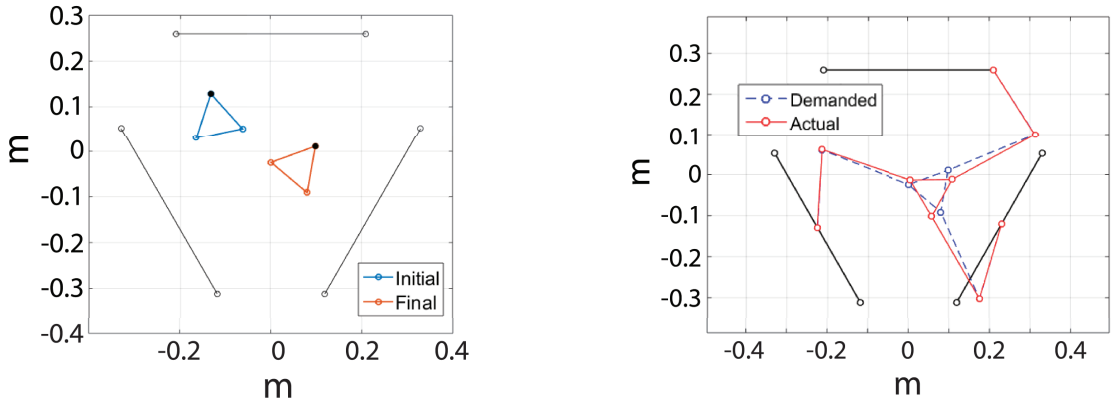

(a) Initial and final positions (demanded)

(b) Final error resulted with Truncated Optimization

Figure 3: Positions depicted within robot workspace

response has been evaluated under a disturbance torque of -0.3 N.m applied at the end-effector (its directions is towards the singularity). The final position of the imposed movement under the presence of this disturbance is shown in Fig. 3b. Since the manipulator loses rigidity, the manipulator fails to deliver a satisfactory response.

The Inverse Kinematic Resolution described in Section 4.2 may be used in order to overcome this problem. Using a convenient ϕ, the manipulator is able to maintain high rigidity. Numerical results show that, under the same disturbance, the final position has been reached satisfactorily. However, the required torques to perform this motion exceed feasible values. In fact, the active prismatic joints demand forces near to 1000N, as depicted by Fig. 4, while the actual prototype can deliver 500N.

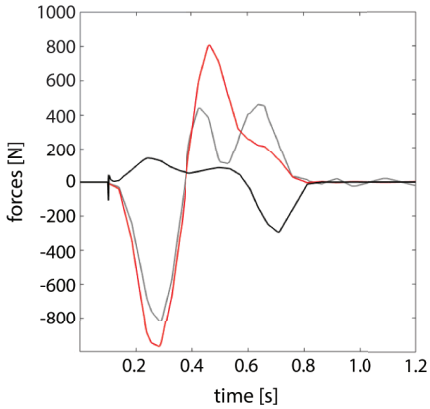

Figure 4: Forces demanded by linear actuators using the Inverse Kinematic Resolution (numerical results)

Finally, the Global Optimization strategy is exploited. With this global approach, the resulting motion can maintain high rigidity without demanding excessive accelerations. Figure 5 demonstrates that the final motion follows the reference motion compromising with its accelerations.

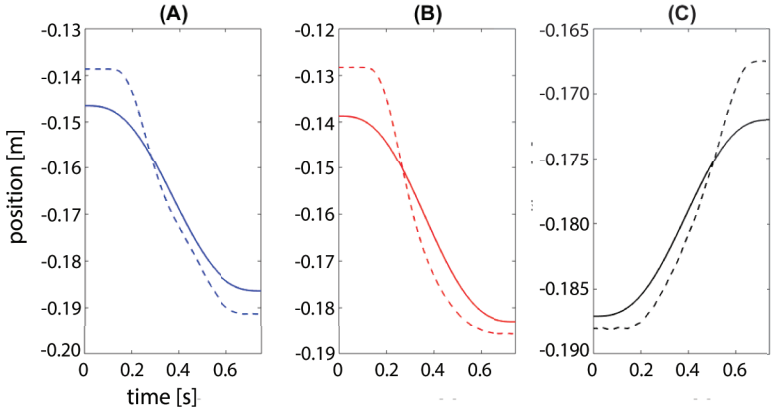

Figure 5: Reference and final positions of (A) ζ_1, (B) ζ_2 and (C) ζ_3 using Global Optimization strategy

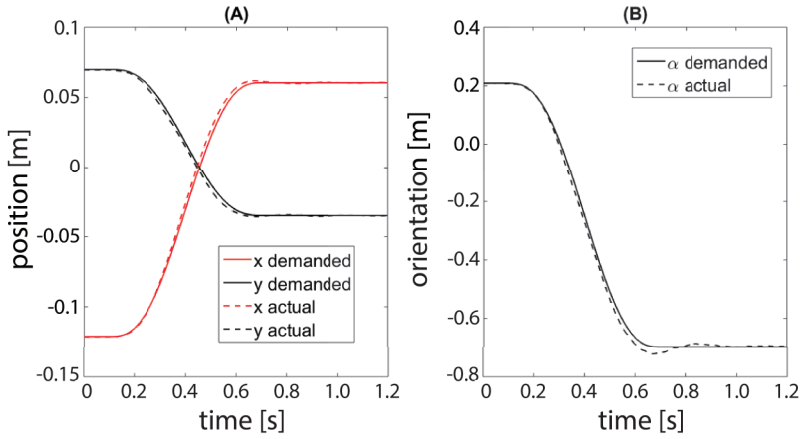

Figure 6: Demanded and actual end-effector positions obtained through experimental test

Using the Global Optimization strategy to plan the use of kinematic redundancy in a satisfactory way, the inputs of the active joints have been calculated and experimentally evaluated. These inputs have been treated accordingly by the controller EPOS using the *Interpolated Position Mode*. During the actual motion, the encoder angular positions and currents have been acquired. These data have been used to calculate the pose of the end-effector via the forward kinematics (see Section 3.1.1). The comparison between the demanded and the actual end-effector poses is shown in Fig. 6. In addition, forces and torques can be estimated through the measured currents. The comparison between the predicted and measured forces and torques is depicted in Fig. 7. A good agreement between the curves can be verified. Details on the parameter identification of this model can be found in (Vieira et al., 2017).

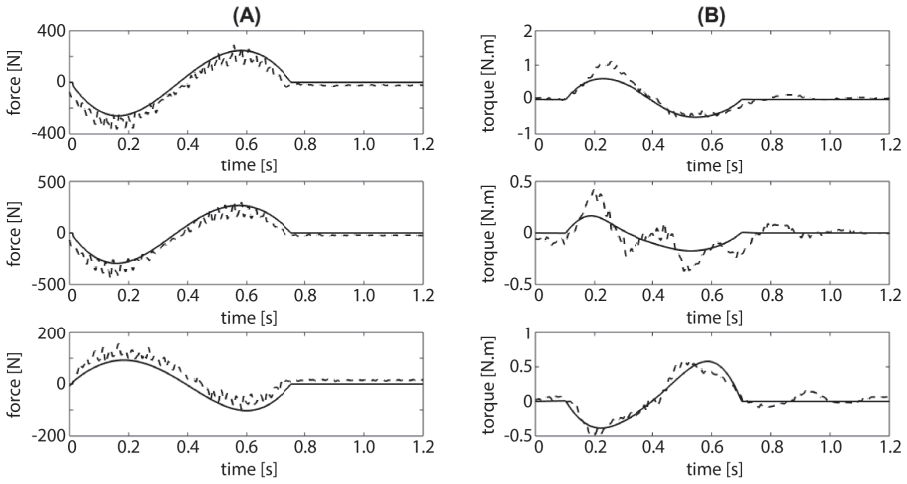

Figure 7: (A) Forces and (B) torques predicted (continuous line) and measured (dashed line)

6. CONCLUSIONS

Three different motion planning strategies were introduced, applied and compared using a mathematical model and physical prototype. Since input variables were just initial and final positions, the truncated optimization turned out to be insufficient for the proposed task. The inverse kinematic resolution presented higher rigidity, although, demanded excessive accelerations. Finally, the proposed global optimization is able to conciliate these two contradictory effects. Simulations showed a promising performance and experimental tests validated the procedure.

Despite of the validity, results indicate that greater efforts on modeling and control strategies are needed. Therefore, friction and dumping may be introduced in the model, and further control strategies considering the interaction between actuators should be applied.

7. ACKNOWLEDGEMENTS

This research is supported by FAPESP 2014/01809-0 and FP7-EMVeM (Energy Efficiency Management for Vehicles and Machines). Moreover, João C. Santos is grateful for his grant FAPESP 2014/21946-2.

8. REFERENCES

Agrawal, O. P. and Xu, Y. (1994). On the global optimum path planning for redundant space manipulators. *IEEE Transactions on Systems, Man and Cybernetics*, 24(9):1306–1316.

Ahuactzin, J. M. and Gupta, K. K. (1999). The kinematic roadmap: a motion planning based global approach for inverse kinematics of redundant robots. *IEEE Transactions on Robotics and Automation*, 15(4):653–669.

Brenan, K. E., Campbell, S. L., and Petzold, L. R. (1996). *Numerical solution of initial-value problems in differential-algebraic equations*, volume 14. Siam.

Fontes, J. V. and da Silva, M. M. (2016). On the dynamic performance of parallel kinematic manipulators with actuation and kinematic redundancies. *Mechanism and Machine Theory*, 103:148–166.

Fontes, J. V. C., Santos, J. C., and da Silva, M. M. (2014). Torque optimization of parallel manipulators by the application of kinematic redundancy. In *Confer{ê}ncia Nacional de Engenharia Mec{â}nica*, Uberlandia, Brazil.

Hairer, E. and Wanner, G. (1996). Solving ordinary differential equations ii: Stiff and differential-algebraic problems second revised edition with 137 figures. *Springer series in computational mathematics*, 14.

Kazerounian, K. and Wang, K. (1988). Global versus local optimization in redundancy resolution of robotic manipulators. *International Journal of Robotics Research*, 7(5):3–12.

Mayne, D. (1966). A second-order gradient method for determining optimal trajectories of non-linear discrete-time systems. *International Journal of Control*, 3(1):85–95.

Merlet, J.-P. (2012). *Parallel robots*, volume 74. Springer Science & Business Media.

Ozgoren, M. K. (2013). Optimal Inverse Kinematic Solutions for Redundant Manipulators by Using Analytical Methods to Minimize Position and Velocity Measures. *Journal of Mechanisms and Robotics*, 5(3):31009.

Santos, J. C., Frederice, D., Fontes, J. V. C., and da Silva, M. M. (2015). Numerical Analysis and Prototyping Details of a Planar Parallel Redundant Manipulator. In *12th Latin American Robotics Symposium, LARS 2015*.

Siciliano, B. (1990). Kinematic control of redundant robot manipulators: A tutorial. *Journal of intelligent and robotic systems*, 3(3):201–212.

Tassa, Y., Erez, T., and Todorov, E. (2012). Synthesis and stabilization of complex behaviors through online trajectory optimization. In *Intelligent Robots and Systems (IROS), 2012 IEEE/RSJ International Conference on*, pages 4906–4913. IEEE.

Vieira, H. L., Santos, J. C., Fontes, J. V. C., and da Silva, M. M. (2017). Dynamic Modelling and Identification of a Planar PKM with Several Levels of Kinematic Redundancy. In *XVII International Symposium on Dynamic Problems of Mechanics - DINAME 2017*, São Sebastião.

Xiang, J., Zhong, C., and Wei, W. (2010). General-weighted least-norm control for redundant manipulators. *IEEE Transactions on Robotics*, 26(4):660–669.

RESPONSIBILITY NOTICE

The authors are the only responsible for the material included in this paper.